13,06

Potential energy surface and energy levels for OH valence vibrations in ferroelectric KH_2PO_4 from basic calculations

© V.A. Abalmasov

S.L. Sobolev Institute of Mathematics,
Novosibirsk, Russia

E-mail: v.a.abalmasov@math.nsc.ru

Received November 12, 2025
Revised December 10, 2025
Accepted December 10, 2025

Hydrogen-bonded ferroelectrics are distinguished by two stable positions of the hydrogen atom along the bond, corresponding to different signs of ferroelectric polarization. In this paper, the potential energy surface for a hydrogen atom along the hydrogen bond in KH_2PO_4 (KDP) is calculated using density functional theory (DFT) at fixed positions of other lattice atoms corresponding to the ferroelectric phase. This potential has one minimum and is strongly asymmetric for the mode A_1, in contrast to the two-well potential calculated at the relaxed positions of the lattice atoms. The excitation energy for hydrogen atoms in this potential is close to the frequencies of OH valence vibrations obtained using DFT in the harmonic approximation, the sufficiency of which for light atoms, however, is not obvious in advance. As a result, the frequencies change in a similar way during deuteration, which is consistent with experimental data. At the same time, the frequencies of OH valence vibrations soften under pressure, which is very unusual and reflects the presence of two stable proton positions along the bond. These results can be applied to other materials with hydrogen bonds.

Keywords: hydrogen bonds, OH valence vibrations, potential energy surface, ferroelectrics, KH_2PO_4.

DOI: 10.61011/PSS.2025.12.63089.8772-25

1. Introduction

Hydrogen bonds are widespread in nature, they bind atoms in a wide variety of substances — from water to complex organic molecules [1,2]. If identical atoms are bound, for example, two oxygen atoms, and the interaction with other atoms is not taken into account, the potential energy surface of the hydrogen atom along the bond is symmetrical with respect to the center of the O−H. . .O bond. Depending on the R_{OO} bond length (i. e., the distance between two oxygen atoms), the potential has one or two minima [3]. The latter case corresponds to hydrogen-bonded ferroelectrics having relatively large values of $R_{OO} \approx 2.5$ Å, and one of the most well-known examples is KH_2PO_4 (KDP), which is widely used for controlling and modulating the frequency of laser radiation. radiation in optoelectronic devices [4,5].

In the paraelectric (PE) phase with the spatial symmetry group $I42d$ (D_{2d}^{12}) [6], which in KDP is above the phase transition temperature of $T_c = 122$ K, protons (nuclei of hydrogen atoms) are randomly distributed with equal probability between two positions along the hydrogen bond lying in the planes xy [6]. All protons occupy only those positions that are closer to the upper (or lower) oxygen atoms of phosphate tetrahedra in the ferroelectric (FE) phase with the spatial symmetry group $Fdd2$ (C_{2v}^{19}), whereas the K, P, and O atoms are shifted along the z axis, which leads to macroscopic upward (or downward) polarization [6,7], see Figure 1.

The frequencies of the hydrogen modes in KDP are higher than the frequencies of other optical phonons due to the low mass of the hydrogen atom. There is a generally accepted opinion that two narrow bands with frequencies (or, more precisely, wavenumbers) 1000 and 1300 cm^{-1} correspond to deformation OH vibrations outside and in the plane (of hydrogen bonds), respectively [8]. Three broad bands are clearly visible in the range of OH valence vibrations, obtained using infrared

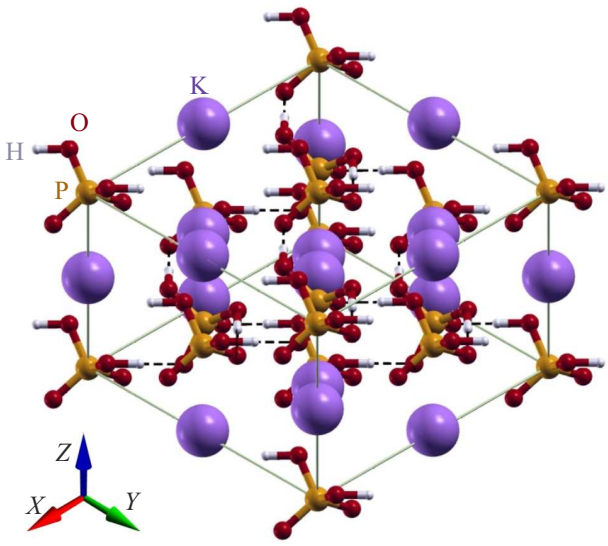

Figure 1. A lattice cell of a KDP crystal in a ferroelectric phase. The large purple, small white, medium orange, and red spheres represent the atoms K, H, P, and O, respectively. The black dotted lines correspond to hydrogen bonds between two neighboring oxygen atoms in the xy plane.

(IR) [9–13], raman scattering (RS) of light [8,14–16] and neutron spectroscopy [17–20] at frequencies around 1800, 2400 and 2700 cm^{-1}. The nature of this triplet, typical for many materials with hydrogen bonds, is usually attributed to the Fermi resonance of the basic OH valence vibrations and overtones and combinations of deformation OH vibrations [21,22], the contribution of which to experimental lines can be determined by dependence on pressure [20].

Initially, it was assumed that the splitting of the band $2400-2700\,cm^{-1}$ was caused by proton (or deuteron) tunneling, and the hydrogen bond potential was approximated by the symmetric double harmonic potential [9]. This idea was further developed using a more realistic double Morse potential along the hydrogen bond, the parameters of which were obtained from the best possible correspondence with the available spectroscopic data [7,23–26]. However, this approach cannot explain why splitting also exists in the FE phase, where there is no proton tunneling, as well as the absence of a strong temperature dependence of the intensity of these modes [24]. The splitting was also attributed to a possible asymmetry of the hydrogen bond potential itself [10,27], while a more exotic and perhaps less likely explanation involves proton tunneling between bonds [28,29]. The relationship of proton motion along the hydrogen bond with the electric dipole moments of distorted tetrahedra PO_4, leading to an asymmetric potential for protons along the bond, was also considered [30–32].

Later, the parameters of the two-well potential were calculated using density functional theory (DFT) [33–40]. However, this potential was not used to calculate the frequencies of OH valence vibrations. Instead, optical phonon frequencies were calculated using density functional perturbation theory (DFPT) [20] or a combination of DFT and frozen phonon method [41–43]. The obtained frequencies of OH valence vibrations turn out to be close to the two upper bands of the three measured in experiments [8–20] and those given above. At the same time, in these calculations, all atomic vibrations are considered only in the harmonic approximation, which may not be sufficient for light nuclei of hydrogen atoms having a relatively large quantum localization length.

In this paper, we calculate the potential energy surface (PES) for OH valence vibrations in KDP at fixed positions of all other lattice atoms using DFT. This approach is close to the standard calculation of phonon modes in the framework of DFT, but it allows taking into account anharmonic effects that should be significant for OH valence vibrations. We show that, despite the asymmetry of the single-well potential obtained in this way, the low-lying energy levels in it are close to the energy levels in its harmonic approximation and, thus, scale in a similar way during deuteration. At the same time, the corresponding phonon frequencies soften with pressure, reflecting the presence of a symmetrical two-well PES in the case of a non-coaxial lattice.

2. Ab initio calculations

The (*ab initio*) calculations were performed using the Quantum Espresso (QE) package [44,45]. The Perdew *et al.* generalized gradient approximation (GGA) (PBE) was used for the exchange-correlation potential [46]. Perhaps less accurate, the local density approximation (LDA) was used only to calculate the Raman (RS) activity, which cannot be obtained with GGA in QE. Valence electrons were represented by pseudopotentials of projector augmented-waves (PAW), and integral sampling in the Brillouin zone (BZ) $4\times4\times4$ was performed using a grid of k-points according to the Monkhorst–Pack scheme [47], which turned out to be sufficient to obtain convergent results. The cutoff energy for structural optimization and energy calculations was 800 eV. The orthorhombic crystal structure of the FE phase at zero temperature with the space group $Fdd2$ (C_{2v}^{19}) and two formula units in a primitive cell was optimized while maintaining crystal symmetry. The Wyckoff positions from Ref. [48] were used as the initial values of the atomic coordinates (see Table A1). The obtained lattice and hydrogen bond parameters (see Table A2) are close to the values from the initial calculations [41] obtained using QE for the same exchange-correlation functional of PBE, and are among the closest parameters to the experimental data [6] among those calculated using various software packages and functions [41]. The optimized atomic positions of the primitive cell are given in Table П3. Reasonable variation of the energy cutoff parameters during the calculation, as well as the use of a denser grid of k-points and other initial positions of atoms before optimizing the lattice, change the final structural parameters and phonon frequencies only by fractions of a percent.

3. Results and discussion

We calculate the frequencies of the OH valence vibration modes in the center of the Brillouin zone (BZ) (see Table) and the corresponding atomic displacements (Figure 2) using the DFPT method implemented in the framework of QE. The calculated frequencies of OH valence vibrations lie in the range of $2230-2440\,cm^{-1}$ (in GGA), depending on their symmetry and propagation vector (see Table), which is close to the values obtained in Refs. [42,43]. To calculate the frequency of longitudinal oscillations ν_{LO}, the dielectric constant tensor and effective Born charges are calculated, and then the phonon frequency is calculated with a small wave vector in the direction of phonon polarization. In the case of LDA, the frequencies of transverse optical (TO) phonons are lower, but the frequencies of longitudinal optical (LO) phonons are the same as in the case of GGA. It should be noted that the modes of OH valence vibrations A_1, B_1 and B_2 (Figure 2) retain the value of the proton charge on the phosphate tetrahedron at any atomic displacement. Mode A_2, which corresponds to the formation of a high-energy Takagi defect at large atomic displacements [38], would change this charge to two proton charges. This may explain its significantly higher frequency. The mode A_1 corresponds to the motion of hydrogen atoms in a ferroelectric soft mode.

Similar calculations of the phonon spectrum in the FE phase of water ice XI, in which the modes of

OH valence vibrations are known to be in the range of 3100–3400 cm^{-1} [49–51], give frequencies lower by about 150 cm^{-1}, which may be related to the PBE functionality that we used, compared to calculations with RPBE [51], PBE0 [52] and meta-GGA functionals [53]. Considering this, it can be expected that the calculated frequencies in the KDP in the table can be increased by the same 150 cm^{-1}, which will bring them closer to the two upper bands of the experimentally observed phonon triplet [8–20], the frequencies of which are indicated above. At the same time, it is difficult to directly compare the frequencies of the OH valence vibration modes (table) with experimental data, where the corresponding bands are very wide.

It should be noted that all protons moving in the mode A_1 experience the same potential landscape at any displacement (see Figure 2), whereas in the modes B_1, B_2 and A_2 this is true only in the harmonic approximation. Therefore, we are building PES primarily for the mode A_1. To do this, we move four hydrogen atoms in the lattice cell along the vector $\mathbf{R}_{OH}$ connecting covalently bonded oxygen and hydrogen atoms. This vector practically coincides with the displacement vectors of protons in the modes of OH valence vibrations, whereas the displacements of other atoms in them are negligible (see Figure A1 and Table A4). This is attributable to the large mass difference between the hydrogen atom and the rest of the lattice atoms.

By relaxing the lattice at each position of the protons δ along the hydrogen bond, we obtain a two-well potential $V_R(\delta)$, which is well approximated by the eighth-order polynomial

$$P_8(\delta-\delta_0)=\sum_{k=0}^{4}c_k(\delta-\delta_0)^{2k}$$

with the distance between the two minima $2\delta_0 \approx 0.424$ Å, See Figure 3 (the coefficients of the polynomial are presented in Table A5). The height of the potential barrier is $V_0 \approx 118$ meV per lattice cell (i. e. four hydrogen atoms), which is close to the value of about 50 meV/KH_2PO_4 obtained in Refs. [36,37].

The frequencies (in units of cm^{-1}) of the transverse (ν_{TO}) and longitudinal (ν_{LO}) OH-valence modes in the center of the BZ along with their IR and RS activity (in units of $D^2\,Å^{-2}\,amu^{-1}$ and $Å^4\,amu^{-1}$, respectively), calculated from first principles (*ab initio*) in two approximations, GGA and LDA. Mode A_1 is polarized along the axis z, B_1 is polarized along the axis y, B_2 is polarized along the axis x [13]. Mode A_2 isnot active in IR spectra

Mode	GGA			LDA			
	ν_{TO}	ν_{LO}	IR	ν_{TO}	ν_{LO}	IR	Raman
B_2	2232	2428	190	2063	2415	239	7.0
B_1	2234	2439	199	2067	2411	232	6.5
A_1	2237	2253	14	2057	2074	10	4.8
A_2	2414	2414	–	2253	2253	–	0.0003

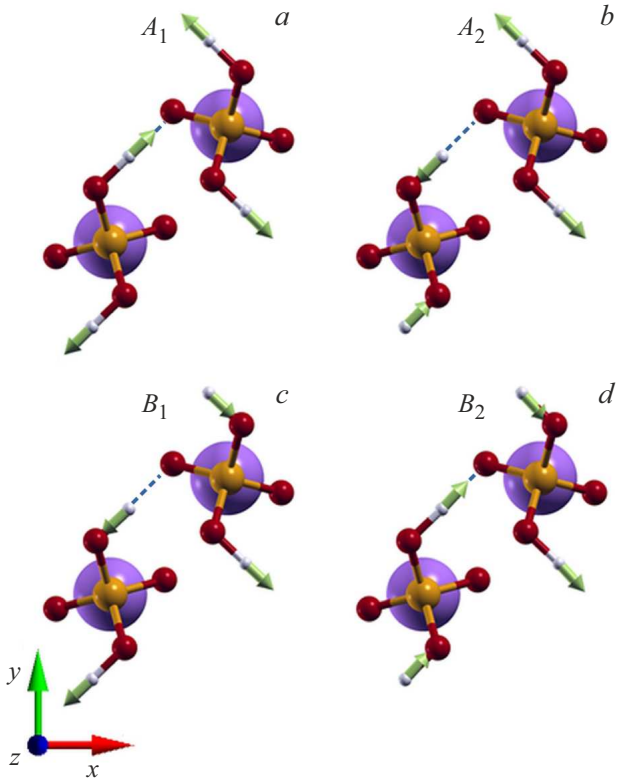

Figure 2. Calculated (*ab initio*) modes of OH valence vibrations in accordance with their irreducible representations. The large purple, small white, medium orange, and red spheres represent the atoms K, H, P, and O, respectively, included in the primitive cell. The arrows show the corresponding atomic displacements. The dotted lines indicate a hydrogen bond.

In the case of a lattice fixed in the FE phase position, which corresponds to $\delta = 0$, the PES $V_F(\delta)$ has one minimum and is asymmetric (Figure 3). We use central finite differences (for the definition and numerical values, see Appendix III and Table A6) to find a numerical approximation of the derivatives $f^{(k)}$ of the potential at its minimum at $\delta = 0$ and to construct Taylor polynomials

$$P_n(\delta)=\sum_{k=2}^{n}f^{(k)}\delta^k/k!$$

of the order of $n = 2$, 4 and 6 (Figure 3). The higher the order of the polynomial, the larger the area in which it approximates the potential $V_F(\delta)$ quite well. Using finite differences, we also construct the Morse potential $V_M(\delta) = D\left(1-e^{-\alpha\delta}\right)^2$, which is believed to provide a good approximation of the covalent bond potential. The parameters of this potential are found as $\alpha = -f^{(3)}/f^{(2)}$ and $D = (f^{(2)})^3/(f^{(3)})^2$. The approximation of $V_F(\delta)$ using $V_M(\delta)$ is comparable to $P_2(\delta)$, but worse than $P_4(\delta)$. We would also like to note that $V_F(\delta)$ for modes B_1, B_2 and A_2 turns out to be very close to the harmonic potential in a wide range of values δ (see Figure A2).

Next, we solve the Schrodinger equation for a particle with a mass of four hydrogen atoms $\mu = 4m_H$

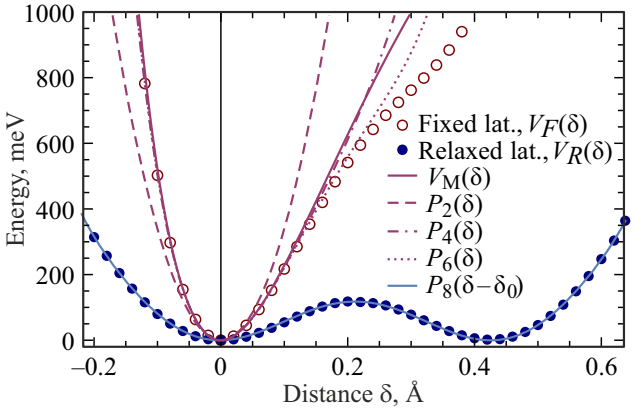

Figure 3. The potential energy surface (PES) for four hydrogen atoms moving in accordance with the mode A_1 of OH valence vibrations at the position of the remaining lattice atoms fixed in the FE phase (empty lilac circles) and de-balanced at each position of the protons (filled blue circles). The PES for a fixed lattice $V_F(\delta)$ is used to find the central differences k of the order to approximate the derivatives $f^{(k)}$ for $\delta = 0$, and then calculate the Morse potential $V_M(\delta)$ (solid lilac line) and Taylor polynomials $P_n(\delta)$ for $n = 2$, 4 and 6 (lilac dashed, dotted, and dotted lines, respectively). The PES with a relaxed lattice $V_R(\delta)$ is well described by the eighth-order polynomial $P_8(\delta - \delta_0)$ with $\delta_0 = 0, 212$ Å (blue solid line).

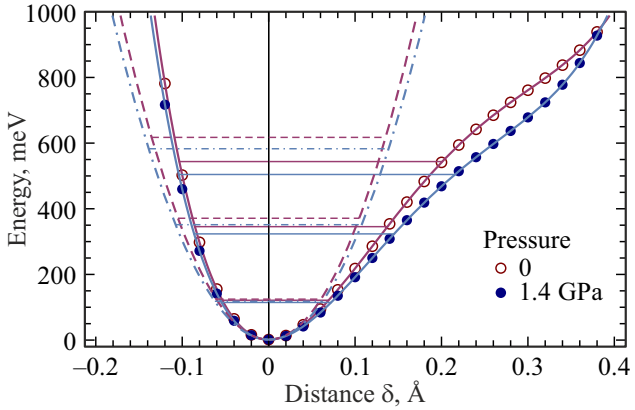

Figure 4. Potential energy surface (PES) $V_F(\delta)$ for four hydrogen atoms moving in accordance with the mode A_1 of OH valence vibrations at the positions of the remaining lattice atoms fixed in the FE phase at zero pressure (empty lilac circles) and at a pressure of 1.4 GPa (filled blue circles). The solid lines correspond to the approximation of PES by cubic splines. The three lower energy levels of the four protons in these potentials are shown by horizontal purple and blue lines. The dotted lilac and dotted blue lines correspond to the harmonic approximation of PES at pressures of 0 and 1.4 GPa. The horizontal dotted lilac and dotted blue lines represent the three lower energy levels of four protons in harmonic potentials at pressures of 0 and 1.4 GPa, respectively.

in the potential $V_F(\delta)$, which is interpolated by cubic splines. The energy difference between the first excited state and the ground state, $\Delta E = E_1 - E_0$, for $V_F(\delta)$ is 225 meV (1813 cm^{-1}), whereas for the harmonic approximation $V_H(\delta) = P_2(\delta)$ it is slightly larger and is 247 meV (1993 cm^{-1}). The latter value also follows directly from the second derivative of the potential, $\Delta E = \hbar\sqrt{f^{(2)}\mu^{-1}}$, and is less than the corresponding phonon frequency of 2237 cm^{-1} (see Table), which may be related to the approximation we made with respect to the mass of the mode and the displacement vector. Although the asymmetric potential $V_F(\delta)$ significantly differs from its harmonic approximation $V_H(\delta)$, the difference in energy levels in both cases is not too great (see Figure 4). As a result, the scaling of the excitation energy of about 1/1.38 during deuteration for $V_F(\delta)$ is close to the scaling of $\sqrt{m_H/m_D} = 1/\sqrt{2}$ for the harmonic potential, which is actually observed in the experiment in Ref. [14].

Interestingly, the excitation energy in the potential $V_F(\delta)$ decreases when external pressure is applied and has the value of $\Delta E = 1690\ cm^{-1}$ at pressure of $P = 1.4$ GPa (this pressure corresponds to experimental data in Ref. [20], see Figure 4. This would be expected for a two-well potential, in which the barrier between two minima decreases under pressure, and the second derivative of the potential at each minimum becomes lower [20]. It turns out that the potential $V_F(\delta)$ obtained with a fixed lattice is actually the sum of the potential $V_R(\delta)$ with a non-aligned lattice and a linear function of δ in the interval between $\delta = 0$ and $\delta = 2\delta_0$ (see Figure A3). The latter may be due to the interaction of protons with distorted electric dipoles of PO_4 tetrahedra, as discussed in Refs. [30–32]. However, beyond the above range, the difference abruptly becomes very large.

Finally, we note that the intensities of IR and RS of the highest frequency mode A_2 are zero (see table), and in order for it to correspond to the highest frequency mode of the phonon triplet observed in the experiment, it must be strongly mixed with other modes of OH valence vibrations. It would also be interesting to investigate the anharmonic potential of OH valence vibration modes experimentally using recently developed methods of pumping and sounding phonons [54].

4. Conclusion

We have shown that the potential energy surface calculated for four hydrogen atoms moving in accordance with the mode A_1 of OH valence vibrations at fixed positions of other atoms in the lattice is strongly asymmetric and one-dimensional. The proton energy levels in this potential and its harmonic approximation are close in values and scale in a similar way during deuteration, which is consistent with experimental data. Despite the fact that the potential has a single minimum, the energy levels in it decrease under external pressure, which reflects the presence of two stable positions of the hydrogen atom along the hydrogen bond. The obtained results can be applied to other materials with hydrogen bonds.

Acknowledgments

The author is grateful to the Siberian Supercomputing Center of the Siberian Branch of the Russian Academy of Sciences (SB RAS) for providing supercomputing equipment.

Funding

The work was performed within the framework of the state assignment of the S.L. Sobolev Institute of Mathematics of SB RAS, project No. FWNF-2022-0021.

Conflict of interest

The authors declare that they have no conflict of interest.

Annex I. Structural parameters of KDP from ab initio calculations

Table A1. Wyckoff's initial positions for atoms from Ref. [48]

Atom	Wyckoff's position	x	y	z
K	8a	0	0	0.519
P	8a	0	0	0
H	16b	0.039	0.183	0.134
O_1	16b	0.133	0.281	0.135
O_2	16b	0.218	0.136	0.385

Table A2. Calculated from the (*ab initio*) parameters of the conditional lattice cell a, b and c, and distances between two oxygen atoms along the hydrogen bond R_{OO}, between covalently bound oxygen and hydrogen atoms R_{OH} and between two stable positions of the hydrogen atom $\delta = R_{OO} - 2R_{OH}$. Experimental data for KDP crystal and deuterated DKDP crystal in ferroelectric phase (at temperature 10–20 K below T_c and atmospheric pressure) are taken from Ref. [6]

Distance (Å)	Calculations	KDP	DKDP
a	10.7961	10.5459	10.5980
b	10.7009	10.4664	10.4959
c	7.0669	6.9265	6.9608
R_{OO}	2.5164	2.4974	2.5332
R_{OH} (R_{OD})	1.0536	1.0564	1.0307
δ	0.4095	0.3846	0.4719

Table A3. Energy-optimized atomic positions in crystallographic coordinates

Atom	a	b	c
K	0.5183307548	0.4816692452	0.5183307548
K	0.7683307548	0.7316692452	0.7683307548
P	−0.0003963357	0.0003963357	−0.0003963357
P	0.2496036643	0.2503963357	0.2496036643
H	0.9905725693	0.0881269307	0.2786683481
H	0.2786683481	0.6426321518	0.9905725693
H	0.6073678482	0.9713316519	0.1618730693
H	0.1618730693	0.2594274307	0.6073678482
O1	0.9864502249	0.2817566985	0.2805475839
O1	0.2805475839	0.4512454926	0.9864502249
O1	0.7987545074	0.9694524161	0.9682433015
O1	0.9682433015	0.2635497751	0.7987545074
O2	0.4705782655	0.9677318236	0.3022485891
O2	0.3022485891	0.2594413219	0.4705782655
O2	0.9905586781	0.9477514109	0.2822681764
O2	0.2822681764	0.7794217345	0.9905586781

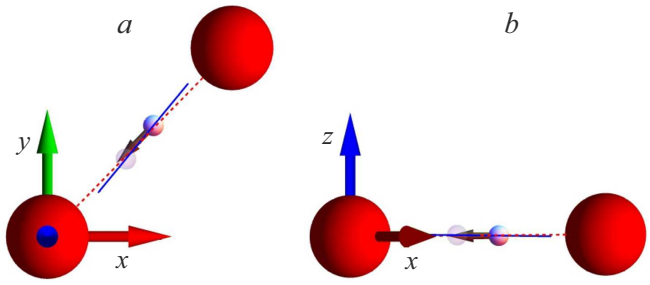

Figure A1. Hydrogen bond between two oxygen atoms, shown by large red spheres. The hydrogen atom is indicated by a small white sphere. The transparent white sphere indicates the alternative stable position of the hydrogen atom. The blue line passes through both positions of the hydrogen atom and corresponds to the vector $\mathbf{R}_{HH}$. The dotted red line connects two oxygen atoms and corresponds to the vector $\mathbf{R}_{OO}$. The angle between these two vectors is about 5 degrees. Brown arrow — displacement of the hydrogen atom in the OH valence mode, which practically coincides with $\mathbf{R}_{OO}$. *a* Projection onto a plane xy. *b* Projection onto a plane containing the axis z and a hydrogen bond.

Appendix II. Atomic displacements in the mode A_1 of OH valence vibrations

Table A4. Calculated (*ab initio*) displacement vector of atoms in the mode A_1 of OH valence vibrations, normalized by one. Hydrogen atoms are covalently bonded to oxygen atoms O_2

Atom	Δx	Δy	Δz
K	0.0000	0.0000	0.0011
K	0.0000	0.0000	0.0011
P	0.0000	0.0000	−0.0156
P	0.0000	0.0000	−0.0156
H	0.3539	0.3509	−0.0039
H	−0.3539	−0.3509	−0.0039
H	0.3539	−0.3509	−0.0039
H	−0.3539	0.3509	−0.0039
O1	0.0107	0.0022	0.0081
O1	−0.0107	−0.0022	0.0081
O1	0.0107	−0.0022	0.0081
O1	−0.0107	0.0022	0.0081
O2	−0.0272	0.0233	0.0059
O2	0.0272	−0.0233	0.0059
O2	−0.0272	−0.0233	0.0059
O2	0.0272	0.0233	0.0059

Annex III. Definition and parameters of polynomials

Table A5. Coefficients of the polynomial $P_8(\delta-\delta_0) = \sum_{k=0}^{4} c_k(\delta-\delta_0)^{2k}$ with $\delta_0 = 0.212$ Å

c_0	$1.18 \cdot 10^2$ meV
c_1	$-5.90 \cdot 10^3$ meV Å^{-2}
c_2	$9.02 \cdot 10^4$ meV Å^{-4}
c_3	$-4.22 \cdot 10^5$ meV Å^{-6}
c_4	$8.00 \cdot 10^5$ meV Å^{-8}

The expression for the central finite difference of the n-th order at the point δ_0 for even n:

$$f^{(n)}(\delta_0) = \sum_{k=0}^{n}(-1)^k C_n^k f(\delta_0 + (n/2-k)h)/h^n, \qquad (A1)$$

where $C_n^k = n!/k!/(n-k)!$ is the binomial coefficient, h is the deviation from the point δ_0.

The average value of $f^{(n)}(\delta_0 - h/2)$ and $f^{(n)}(\delta_0 + h/2)$ is taken for odd n .

Table A6. Numerical values for the central differences for constructing polynomials $P_n(\delta) = \sum_{k=2}^{n} f^{(k)}\delta^k/k!$ for $n = 2$, 4 and 6 for $\delta_0 = 0$, $h = 0.02$ Å

$f^{(2)}$	$6.73 \cdot 10^4$ meV Å^{-2}
$f^{(3)}$	$-8.44 \cdot 10^5$ meV Å^{-3}
$f^{(4)}$	$5.69 \cdot 10^6$ meV Å^{-4}
$f^{(5)}$	$-2.97 \cdot 10^7$ meV Å^{-5}
$f^{(6)}$	$2.98 \cdot 10^8$ meV Å^{-6}

Annex IV. Potential energy surface for all modes of OH valence vibrations

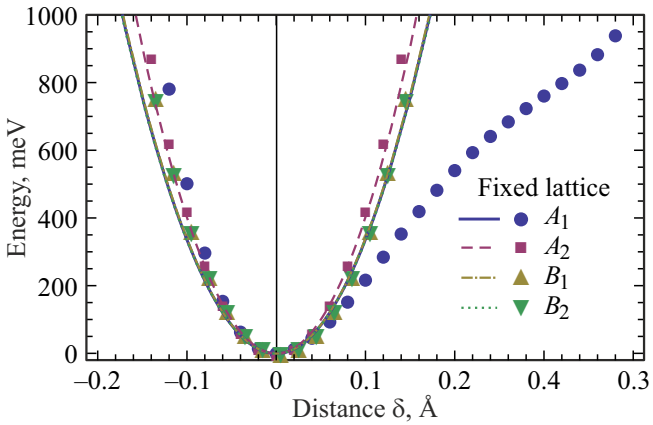

Figure A2. Potential energy surface (PES) for four hydrogen atoms moving according to the modes of OH valence vibrations at the positions of the remaining lattice atoms fixed in the ferroelectric phase. The obtained potential $V_F(\delta)$ was used to find the central finite difference of the second order $f^{(2)}$ to approximate the second-order derivative and then the Taylor polynomial $P_2(\delta) = f^{(2)}\delta^2/2!$ for each mode of the OH valence vibration.

Appendix V. Potential difference with fixed and non-aligned positions of lattice atoms for mode A_1 of OH vibrations

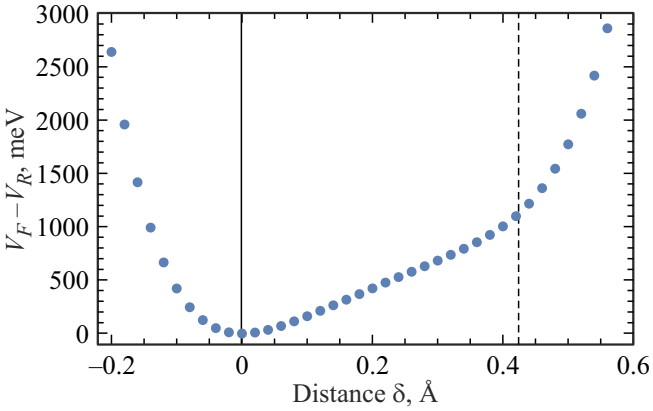

Figure A3. Difference between the potentials for four hydrogen atoms moving according to the mode A_1 of OH valence vibrations along the vector $\mathbf{R}_{OH}$, at fixed positions of the remaining lattice atoms in the ferroelectric phase, $V_F(\delta)$, and at the relaxed positions of the lattice atoms, $V_R(\delta)$. The solid vertical line corresponds to the position of the hydrogen atom in the ferroelectric phase. The dotted vertical line corresponds to the stable position of the hydrogen atom in the ferroelectric phase with the opposite ferroelectric polarization. The dependence on δ is close to linear between two vertical lines.

References

[1] G.A. Jeffrey, W. Saenger. Hydrogen Bonding in Biological Structures. Springer, Berlin-Heidelberg (1991).
[2] S.J. Grabowski, ed. Hydrogen Bonding — New Insights. Springer, Dordrecht, Netherlands (2006).
[3] A. Novak. In: Large Molecules. Structure and Bonding, Vol. 18. Springer, Berlin-Heidelberg (1974). pp. 177–216.
[4] R.-B. Jin, N. Cai, Y. Huang, X.-Y. Hao, S. Wang, F. Li, H.-Z. Song, Q. Zhou, R. Shimizu. Phys. Rev. Appl. **11**, 034067 (2019).
[5] S.Y. Mironov, I.B. Mukhin, V.V. Lozhkarev, A.K. Potemkin, M.A. Martyanov, I.V. Kuzmin, E.A. Khazanov. Appl. Opt. **61**, 6033 (2022).
[6] R.J. Nelmes, Z. Tun, W.F. Kuhs. Ferroelectrics **71**, 125 (1987).
[7] R.J. Nelmes. Ferroelectrics **71**, 87 (1987).
[8] W. Liu, H. Xia, X. Wang, Z. Ling, J. Xu, Y. Wei, Y. Liu, H. Han, J. Alloys Compd. **430**, 226 (2007).
[9] R. Blinc, D. Had.i. Mol. Phys. **1**, 391 (1958).
[10] Y. Imry, I. Pelah, E. Wiener. J. Chem. Phys. **43**, 2332 (1965).
[11] R.M. Hill, S.K. Ichiki. J. Chem. Phys. **48**, 838 (1968).
[12] F. Gervais, P. Simon. Ferroelectrics **72**, 77 (1987).
[13] P. Simon, F. Gervais, E. Courtens. Phys. Rev. B **37**, 1969 (1988).
[14] Y. Tominaga, Y. Kawahata, Y. Amo. Solid State Commun. **125**, 419 (2003).
[15] Y. Mita, K. Takebe, M. Kobayashi, S. Endo, Y. Tominaga. J. Phys.: Condens. Matter **18**, 5185 (2006).
[16] V.A. Abalmassov, N.V. Surovtsev. Bull. Russ. Acad. Sci.: Phys. **82**, 294 (2018).
[17] K. Shibata, S. Ikeda. J. Phys. Soc. Jpn. **61**, 411 (1992).
[18] K. Mizoguchi, Y. Nakai, S. Ikeda, A. Agui, Y. Tominaga. J. Phys. Soc. Jpn. **62**, 451 (1993).
[19] A.V. Belushkin, M.A. Adams. Phys. B: Condens. Matter **234–236**, 37 (1997).
[20] V.A. Abalmasov, A.S. Ivanov, R.A. Sadykov, A.V. Belushkin. Phys. Rev. B **112**, 214101 (2025).
[21] S. Bratos, H. Ratajczak. J. Chem. Phys. **76**, 77 (1982).
[22] S. Bratos, H. Ratajczak, P. Viot. In: Hydrogen-Bonded Liquids. Springer, Netherlands (1991). pp. 221–235.
[23] M.C. Lawrence, G.N. Robertson. J. Phys. C: Solid State Phys. **13**, L1053 (1980).
[24] M.C. Lawrence, G.N. Robertson. Ferroelectrics **34**, 179 (1981).
[25] G.N. Robertson, M.C. Lawrence. J. Physics C: Solid State Phys. **14**, 4559 (1981).
[26] E. Matsushita, T. Matsubara. Prog. Theor. Phys. **67**, 1 (1982).
[27] F. Fillaux, A. Cousson. Eur. Phys. J. B **89**, 72 (2016).
[28] C.A. Cody, R.K. Khanna. Ferroelectrics **9**, 251 (1975).
[29] R.K. Khanna, M.-H. Sun. Ferroelectrics **29**, 209 (1980).
[30] H. Sugimoto, S. Ikeda. Phys. Rev. Lett. **67**, 1306 (1991).
[31] S. Ikeda, H. Sugimoto, Y. Yamada. Phys. Rev. Lett. **81**, 5449 (1998).
[32] D. Merunka, B. Rakvin. Phys. Rev. B **76**, 140101 (2007).
[33] Y.G. Hao, X.Y. Sun, N.S. Dalal. Ferroelectrics **132**, 165 (1992).
[34] B. Silvi, Z. Latajka, H. Ratajczak. Ferroelectrics **150**, 303 (1993).
[35] Q. Zhang, F. Chen, N. Kioussis, S.G. Demos, H.B. Radousky. Phys. Rev. B **65**, 024108 (2001).
[36] S. Koval, J. Kohanoff, R.L. Migoni, E. Tosatti. Phys. Rev. Lett. **89**, 187602 (2002).
[37] S. Koval, J. Kohanoff, J. Lasave, G. Colizzi, R.L. Migoni. Phys. Rev. B **71**, 184102 (2005).
[38] J. Lasave, S. Koval, N.S. Dalal, R. Migoni. Phys. Rev. B **72**, 104104 (2005).
[39] J. Lasave, J. Kohanoff, R.L. Migoni, S. Koval. Phys. B: Condens. Matter **404**, 2736 (2009).
[40] S. Koval, J. Lasave, J. Kohanoff, R. Migoni. Ferroelectrics **401**, 103 (2010).
[41] R. Menchón, G. Colizzi, C. Johnston, F. Torresi, J. Lasave, S. Koval, J. Kohanoff, R. Migoni. Phys. Rev. B **98**, 104108 (2018).
[42] C.-L. Jiang, W. Zeng, N. Yang, F.-S. Liu, B. Tang, Q.-J. Liu. Optik **223**, 165645 (2020).
[43] E.A. Engel. J. Chem. Phys. **148**, 144708 (2018).
[44] P. Giannozzi, S. Baroni, N. Bonini, M. Calandra, R. Car, C. Cavazzoni, D. Ceresoli, G.L. Chiarotti, M. Cococcioni, I. Dabo, A.D. Corso, S. de Gironcoli, S. Fabris, G. Fratesi, R. Gebauer, U. Gerstmann, C. Gougoussis, A. Kokalj, M. Lazzeri, L. Martin-Samos, N. Marzari, F. Mauri, R. Mazzarello, S. Paolini, A. Pasquarello, L. Paulatto, C. Sbraccia, S. Scandolo, G. Sclauzero, A.P. Seitsonen, A. Smogunov, P. Umari, R.M. Wentzcovitch. J. Physics: Condens. Matter **21**, 395502 (2009).
[45] P. Giannozzi, O. Andreussi, T. Brumme, O. Bunau, M.B. Nardelli, M. Calandra, R. Car, C. Cavazzoni, D. Ceresoli, M. Cococcioni, N. Colonna, I. Carnimeo, A.D. Corso, S. de Gironcoli, P. Delugas, R.A. DiStasio, A. Ferretti, A. Floris, G. Fratesi, G. Fugallo, R. Gebauer, U. Gerstmann, F. Giustino, T. Gorni, J. Jia, M. Kawamura, H.-Y. Ko, A. Kokalj, E. Küçükbenli, M. Lazzeri, M. Marsili, N. Marzari, F. Mauri, N.L. Nguyen, H.-V. Nguyen, A.O. de-la Roza, L. Paulatto, S. Poncé, D. Rocca, R. Sabatini, B. Santra, M. Schlipf, A.P. Seitsonen, A. Smogunov, I. Timrov, T. Thonhauser, P. Umari, N. Vast, X. Wu, S. Baroni. J. Physics: Condens. Matter **29**, 465901 (2017).
[46] J.P. Perdew, K. Burke, M. Ernzerhof. Phys. Rev. Lett. **77**, 3865 (1996).
[47] H.J. Monkhorst, J.D. Pack. Phys. Rev. B **13**, 5188 (1976).
[48] M. Jia, X. Cheng, M.-H. Whangbo, M. Hong, S. Deng. RSC Adv. **10**, 26479 (2020).
[49] T.K. Hirsch, L. Ojamäe. J. Phys. Chem. B **108**, 15856 (2004).
[50] T. Shigenari, K. Abe. J. Chem. Phys. **136**, 174504 (2012).
[51] P. Zhang, Z. Wang, Y.-B. Lu, Z.-W. Ding. Sci. Rep. **6**, 29273 (2016).
[52] C. J. Burnham, T. Hayashi, R.L. Napoleon, T. Keyes, S. Mukamel, G.F. Reiter. J. Chem. Phys. **135**, 144502 (2011).
[53] J. Xu, M. Chen, C. Zhang, X. Wu. Phys. Rev. B **99**, 205123 (2019).
[54] A. von Hoegen, R. Mankowsky, M. Fechner, M. Först, A. Cavalleri. Nature **555**, 79 (2018).

Translated by A.Akhtyamov